universe

MDPI

Article

Decoupled Embedding Class-One Strange Stars in Self-Interacting Brans–Dicke Gravity †

Muhammad Sharif * and Amal Majid

Department of Mathematics, University of the Punjab, Quaid-e-Azam Campus, Lahore 54590, Pakistan; amalmajid89@gmail.com

* Correspondence: msharif.math@pu.edu.pk

† This paper is an extended version from the proceeding paper: Muhammad Sharif and Amal Majid. Compact Objects in Brans-Dicke Gravity. In Proceedings of the 1st Electronic Conference on Universe: online, 22–28 February 2021.

Abstract: This work aims to extend two isotropic solutions to the anisotropic domain by decoupling the field equations in self-interacting Brans–Dicke theory. The extended solutions are obtained by incorporating an additional source in the isotropic fluid distribution. We deform the radial metric potential to disintegrate the system of field equations into two sets such that each set corresponds to only one source (either isotropic or additional). The system related to the anisotropic source is solved by employing the MIT bag model as an equation of state. Further, we develop two isotropic solutions by plugging well-behaved radial metric potentials in Karmarkar's embedding condition. The junction conditions at the surface of the star are imposed to specify the unknown constants appearing in the solution. We examine different physical characteristics of the constructed quark star models by using the mass and radius of PSR J1903+327. It is concluded that, in the presence of a massive scalar field, both stellar structures are well-behaved, viable and stable for smaller values of the decoupling parameter.

Keywords: quark stars; Brans–Dicke theory; gravitational decoupling

check for updates

Citation: Sharif, M.; Majid, A. Decoupled Embedding Class-One Strange Stars in Self-Interacting Brans–Dicke Gravity. *Universe* **2021**, *7*, 161. https://doi.org/10.3390/universe7060161

Academic Editors: James A. Isenberg, Gerald B. Cleaver, Gonzalo J. Olmo, Lijing Shao and Giacomo Tommei

Received: 29 April 2021
Accepted: 21 May 2021
Published: 24 May 2021

Publisher's Note: MDPI stays neutral with regard to jurisdictional claims in published maps and institutional affiliations.

Copyright: © 2021 by the authors. Licensee MDPI, Basel, Switzerland. This article is an open access article distributed under the terms and conditions of the Creative Commons Attribution (CC BY) license (https://creativecommons.org/licenses/by/4.0/).

1. Introduction

The present-day universe consists of a cosmic web of large-scale structures such as clusters of galaxies and stars. The study of these astronomical objects provides insight into the evolution of the cosmos from its origin to the current cosmic era. In this regard, the study of compact objects born from the collapse of gaseous stars has gained the attention of astrophysicists. The neutron star is an outcome of stellar collapse whose mass lies within the interval $1M_{\odot}$ to $3M_{\odot}$ ($M_{\odot}$ denotes mass of the sun). This celestial object supports itself against further collapse through the degeneracy pressure of neutrons. However, it is hypothesized that a neutron star with a mass exceeding the limit of $3M_{\odot}$ continues to collapse inward. The process of collapse sufficiently increases the temperature and pressure which causes the neutrons to break down into elementary particles known as quarks. This leads to the formation of stable dense quark stars [1]. According to Witten [2], matter composed of hadrons is less stable than the fluid distribution containing strange, up, and down quarks. Further, researchers believe that the presence of strange quark stars provides an explanation regarding the huge emission of radiation from extremely luminous supernovae [3].

A suitable equation of state (EoS) that incorporates the necessary features of quark-gluon plasma is required to describe the mechanism of ultra-dense quark stars. However, a model that can aptly explain the interactions of quarks in the dense cores of strange stars is still under discussion. Researchers have deemed the MIT bag model as the most suitable EoS in the absence of the best fit [4]. The bag constant ($\mathcal{B}$) appearing in the model makes a distinction between true and false vacuum. Moreover, this EoS was used to

estimate the mass of compact quark stars. These predictions match with the statistical results obtained from the cosmic events GW170817 [5] and GW190425 [6] which supports the choice of the MIT bag model. This model has been employed numerous times to examine the physical characteristics of strange stars [7–9]. Arbañil and Malheiro [10] developed a strange star structure using the bag model and checked its stability through radial perturbations. Bhar [11] used this EoS along with the embedding class-one condition to develop anisotropic quark stellar models. Recently, Ferreira and da Rocha [12] discussed the relation between configurational entropy and mass of a family of nucleons.

The relation between matter and geometry of an astrophysical structure is established via the field equations. Thus, the solutions of field equations are required to inspect the important features of celestial systems. Schwarzschild [13] solved these complicated differential equations and obtained the first solution corresponding to an isotropic fluid distribution in general relativity (GR). However, realistic cosmic structures rarely demonstrate isotropic behavior as the composite particles move differently in tangential and radial directions. Thus, anisotropy in pressure must be taken into account while investigating stellar structures. A detailed analysis of source as well as the influence of anisotropy on several physical features (such as mass-radius relation, stability, etc.) of self-gravitating systems was done by Herrera and Santos [14]. Different anisotropic solutions have also been constructed by adopting various methods [15–17]. However, the extraction of stable and well-behaved anisotropic models is still under discussion.

Recently, Ovalle [18] introduced the technique of decoupling via minimal geometric deformation (MGD) which minimizes the degrees of freedom in the system of field equations and facilitates the extension of well-known solutions to more complex domains. According to this scheme, new gravitational sources are successively incorporated in the seed or original matter distribution to include the intricate properties of cosmic objects. The deformation of the radial metric component decouples the two sources by formulating a system of equations corresponding to each matter source. Each system is solved independently and the solutions are combined according to the superposition principle to obtain a solution of the whole system. An important feature of this scheme is that it does not allow the transfer of energy between the two fluid distributions. Ovalle [19] also proposed an extension of MGD scheme by transforming radial as well as temporal metric functions.

The effective scheme of decoupling has been applied to various astrophysical and cosmological solutions to obtain their anisotropic extensions. Isotropic configuration corresponding to Tolman IV was decoupled via MGD and extended to the anisotropic domain in braneworld [20] as well as GR [21]. Viable anisotropic self-gravitating models were constructed by deforming the metric potentials of Durgapal-Fuloria [22], Heintzmann [23], Krori-Barua [24] and Schwarzschild [25] solutions. Contreras [26,27] evaluated the anisotropic version of (2+1)-dimensional spacetime involving the cosmological constant. An isotropic solution was generated through Karmarkar's condition and then extended to anisotropic domain by Singh et al. [28]. The approach of decoupling was also applied to Tolman VII ansatz [29]. Sharif and Ama-Tul-Mughani [30,31] minimally deformed the spacetime related to a cloud of strings to compute anisotropic charged solutions. The technique of MGD has also been applied to cosmological solutions namely, FLRW and Kantowski–Sachs spacetimes [32]. Recently, it was shown that the approach of decoupling can also be applied to axially symmetric spacetimes by formulating anisotropic extension of Kerr metric [33]. The static stellar distributions derived using the method of MGD have also been probed with trace and Weyl anomalies [34].

Dirac's proposal (ratios of cosmological quantities and physical constants produced large dimensionless numbers) provided the motivation behind a dynamical gravitational constant as it referred to an underlying relation between G and cosmic time [35,36]. Brans–Dicke (BD) theory is the simplest scalar-tensor theory that modifies GR to encompass the effects of a varying gravitational constant (G) [37]. The massless scalar field (ϑ) in BD theory is defined as the reciprocal of G. It is coupled to the matter source through a tunable BD coupling parameter (ω_{BD}). The values of this parameter can be adjusted to

explain the early cosmos as well as the late-time acceleration. Moreover, large coupling parameter restricts the role of scalar field in cosmological scenarios. However, the large values of ω_{BD} corresponding to the weak gravitational field [38] do not agree with the range of small values required to explain the inflationary era [39]. This discrepancy is rectified through a modification of BD theory (known as self-interacting BD (SBD) theory) which admits a self-interacting potential function ($V(\sigma)$) and a massive scalar field (σ). Self-interacting BD gravity permits all values of the coupling parameter greater than $-\frac{3}{2}$ for $m_\sigma > 2 \times 10^{-25}$ GeV (m_σ denotes mass of the scalar field) [40].

Different astrophysical phenomena have been discussed in BD as well as SBD gravity. Buchdahl [41] evaluated BD counterparts of axial as well as spherical solutions of GR. Bruckman and Kazes [42] evaluated the form of scalar field corresponding to perfect fluid. Singh and Rai [43] presented a method to formulate stationary axially symmetric solutions of BD Maxwell field equations. Demiański-type metric was obtained through a complex coordinate transformation by Krori and Bhattacharjee [44]. Many researchers have discussed the impact of scalar field on physical features of rapidly as well as slowly rotating neutron stars [45–48]. We have investigated the viability and stability of strange quark stars in the presence of a massive scalar field [49,50]. The scheme of decoupling via MGD has been applied in the context of SBD as well as other modified theories to obtain well-behaved anisotropic spacetimes [51–60].

In this paper, we generate two isotropic spherical structures through embedding class-one condition and extend them to the anisotropic domain via MGD scheme in SBD gravity. The features of extended solutions, developed corresponding to the MIT bag model, are analyzed graphically. We construct the system of field equations involving the additional source in the next section. In Section 3, the field equations are disintegrated through a deformation in the radial metric component. We devise and inspect the anisotropic extensions of solutions obtained via Karmarkar's condition in Section 4. We discuss the main results in Section 5.

2. Self-Interacting Brans–Dicke Theory

The field equations of SBD gravity are obtained by varying the action (in relativistic units)

$$S = \int \sqrt{-g}(\mathcal{R}\sigma - \frac{\omega_{BD}}{\sigma}\nabla^\gamma\nabla_\gamma\sigma - V(\sigma) + \Upsilon L_\Theta + L_m)d^4x, \tag{1}$$

with respect to the metric tensor ($g_{\gamma\delta}$) and are given as

$$G_{\gamma\delta} = \mathcal{R}_{\gamma\delta} - \frac{1}{2}g_{\gamma\delta}\mathcal{R} = T^{(\text{eff})}_{\gamma\delta} = \frac{1}{\sigma}(T^{(m)}_{\gamma\delta} + \Upsilon\Theta_{\gamma\delta} + T^{\sigma}_{\gamma\delta}). \tag{2}$$

Here, the matter Lagrangian of the seed source, Ricci tensor and Ricci scalar are denoted by L_m, $\mathcal{R}_{\gamma\delta}$ and $\mathcal{R}$, respectively whereas L_Θ denotes the Lagrangian related to the anisotropic source (Θ). The decoupling parameter (Υ) governs the influence of the new source that may correspond to a tensor, vector or scalar field. The isotropic source is represented in terms of four-velocity (v_γ), energy density (ρ) and pressure (p) through the following energy-momentum tensor

$$T^{(m)}_{\gamma\delta} = \rho v_\gamma v_\delta + p(v_\gamma v_\delta - g_{\gamma\delta}), \tag{3}$$

whereas $T^{\sigma}_{\gamma\delta}$ measures the impact of scalar field on the physical features of matter distribution and is given as

$$T^{\sigma}_{\gamma\delta} = \sigma_{,\gamma;\delta} - g_{\gamma\delta}\Box\sigma + \frac{\omega_{BD}}{\sigma}(\sigma_{,\gamma}\sigma_{,\delta} - \frac{g_{\gamma\delta}\sigma_{,\alpha}\sigma^{,\alpha}}{2}) - \frac{V(\sigma)g_{\gamma\delta}}{2}, \tag{4}$$

where $\Box\sigma = \frac{1}{\sqrt{-g}}(\sqrt{-g}g^{\gamma\delta}\sigma_{,\gamma})_{,\delta}$. The wave equation of the scalar field is derived from Equation (1) as

$$\Box\sigma = \frac{T^{(m)} + \Upsilon\Theta}{3+2\omega_{BD}} + \frac{1}{3+2\omega_{BD}}(\sigma\frac{dV(\sigma)}{d\sigma} - 2V(\sigma)), \tag{5}$$

where the traces of energy-momentum tensors $T^{(m)}_{\gamma\delta}$ and $\Theta_{\gamma\delta}$ are denoted by $T^{(m)}$ and Θ, respectively. It is worthwhile to mention here that the effective energy-momentum tensor obeys the conservation law, i.e., $T^{(\text{eff})\gamma}_{\delta;\gamma} = 0$.

We obtain the anisotropic extension of the seed source by considering a spherically symmetric interior of the static astrophysical object. The line element describing the spherical geometry reads

$$ds^2 = e^{\xi(r)}dt^2 - e^{\phi(r)}dr^2 - r^2d\theta^2 - r^2\sin^2\theta d\varphi^2. \tag{6}$$

The four-velocity corresponding to the above metric is $v^\gamma = (e^{-\frac{\xi}{2}}, 0, 0, 0)$ while the field equations incorporating the effects of the scalar field, seed and additional sources are expressed as

$$\frac{1}{r^2} - e^{-\phi}\left(\frac{1}{r^2} - \frac{\phi'}{r}\right) = \frac{1}{\sigma}(\rho + \Upsilon\Theta^0_0 + T^{0\sigma}_0), \tag{7}$$

$$-\frac{1}{r^2} + e^{-\phi}\left(\frac{1}{r^2} + \frac{\xi'}{r}\right) = \frac{1}{\sigma}(p - \Upsilon\Theta^1_1 - T^{1\sigma}_1), \tag{8}$$

$$\frac{e^{-\phi}}{4}\left(2\xi'' + \xi'^2 - \phi'\xi' + 2\frac{\xi' - \phi'}{r}\right) = \frac{1}{\sigma}(p - \Upsilon\Theta^2_2 - T^{2\sigma}_2), \tag{9}$$

where

$$\begin{aligned}
T^{0\sigma}_0 &= e^{-\phi}\left[\sigma'' + \left(\frac{2}{r} - \frac{\phi'}{2}\right)\sigma' + \frac{\omega_{BD}}{2\sigma}\sigma'^2 - e^{\phi}\frac{V(\sigma)}{2}\right],\\
T^{1\sigma}_1 &= e^{-\phi}\left[\left(\frac{2}{r} + \frac{\xi'}{2}\right)\sigma' - \frac{\omega_{BD}}{2\sigma}\sigma'^2 - e^{\phi}\frac{V(\sigma)}{2})\right],\\
T^{2\sigma}_2 &= e^{-\phi}\left[\sigma'' + \left(\frac{1}{r} - \frac{\phi'}{2} + \frac{\xi'}{2}\right)\sigma' + \frac{\omega_{BD}}{2\sigma}\sigma'^2 - e^{\phi}\frac{V(\sigma)}{2}\right].
\end{aligned}$$

Here, prime indicates differentiation with respect to the radial coordinate. Moreover, the wave Equation (5) corresponding to metric (6) takes the form

$$\begin{aligned}
\Box\sigma &= -e^{-\phi}\left[\left(\frac{2}{r} - \frac{\phi'}{2} + \frac{\xi'}{2}\right)\sigma' + \sigma''\right]\\
&= \frac{1}{3+2\omega_{BD}}\left[\Theta + T^{(m)} + \left(\sigma\frac{dV(\sigma)}{d\sigma} - 2V(\sigma)\right)\right].
\end{aligned} \tag{10}$$

The field Equations (7)–(9) imply that the extra source induces anisotropy in the system for $\Theta^1_1 \neq \Theta^2_2$.

3. Gravitational Decoupling

In this section, we apply the technique of decoupling to minimize the number of unknowns (state parameters, massive scalar field, metric functions and components of anisotropic source) in the system of field equations. The complex field Equations (7)–(9) are disintegrated into two simpler sets by transforming the metric potentials as

$$\xi(r) \mapsto \chi(r) + \Upsilon\nu(r), \quad e^{-\phi(r)} \mapsto \lambda(r) + \Upsilon\mu(r), \tag{11}$$

where $\nu(r)$ and $\mu(r)$ are the deformation functions that govern the translation in temporal and radial metric components, respectively. In case of MGD scheme, $\nu(r) = 0$, i.e., the transformation is applied on the radial metric potential only while the temporal metric component remains unchanged. Moreover, the symmetry of the spherical structure is unaffected by the linear mapping. The set corresponding to isotropic fluid is obtained by applying the transformation in Equations (7)–(9) and setting $\mathrm{Y} = 0$ to exclude the effect of the anisotropic source. The first set is expressed as

$$\begin{aligned}
\rho &= -\frac{1}{2r^2\sigma(r)}[r^2\omega_{BD}\lambda(r)\sigma'^2(r) - r^2\sigma(r)V(\sigma) + r\sigma(r)(r\lambda'(r)\sigma'(r) + 2r\lambda\sigma'' \\
&+ 4\lambda(r)\sigma'(r)) + 2\sigma^2(r)(r\lambda'(r) + \lambda(r) - 1)], \qquad (12)\\
p &= \frac{1}{r^2}[\sigma(r)(r\lambda(r)\xi'(r) + \lambda(r) - 1)] + \frac{1}{2r\sigma(r)}[\lambda(r)\sigma'(r)(\sigma(r)(r\xi'(r) + 4) \\
&- r\omega_{BD}\sigma'(r))] - \frac{V(\sigma)}{2}, \qquad (13)\\
p &= \frac{1}{4r\sigma(r)}[\sigma(r)\lambda'(r)(\sigma(r)(r\xi'(r) + 2) + 2r\sigma'(r)) + \lambda(r)(2\sigma(r)\sigma'(r) \\
&\times ((r\xi'(r) + 2) + 2r\sigma''(r)) + \sigma^2(r)(2r\xi''(r) + r\xi'^2(r) + 2\xi'(r)) \\
&+ 2r\omega_{BD}\sigma'^2(r)) - 2r\sigma(r)V(\sigma)]. \qquad (14)
\end{aligned}$$

The isotropic source is conserved in the presence of massive scalar field as

$$T_1^{1'(\mathrm{eff})} - \frac{\xi'(r)}{2}(T_0^{0(\mathrm{eff})} - T_1^{1(\mathrm{eff})}) = 0. \qquad (15)$$

The second array is formulated by subtracting Equations (12)–(14) from the system of transformed field equations. The components of the additional source are described by the second set as

$$\begin{aligned}
\Theta_0^0 &= \frac{-1}{2r^2\sigma(r)}[r\sigma(r)\mu'(r)(r\sigma'(r) + 2\sigma(r)) + \mu(r)(r^2\omega_{BD}\sigma'^2(r) + 2r\sigma(r) \\
&\times (r\sigma''(r) + 2\sigma'(r)) + 2\sigma^2(r))], \qquad (16)\\
\Theta_1^1 &= \frac{-1}{2r^2\sigma(r)}[\mu(r)(-r^2\omega_{BD}\sigma'(r)^2 + r\sigma(r)(r\xi'(r) + 4)\sigma'(r) + 2\sigma^2(r) \\
&\times (r\xi'(r) + 1))], \qquad (17)\\
\Theta_2^2 &= \frac{-1}{4\sigma(r)}[2\sigma(r)(r\mu'(r)\sigma'(r) + \mu(r)((r\xi'(r) + 2)\sigma'(r) + 2r\sigma''(r))) \\
&+ \sigma^2(r)(\mu'(r)(r\xi'(r) + 2) + \mu(r)(2r\xi''(r) + r\xi'^2(r) + 2\xi'(r))) \\
&+ 2r\omega_{BD}\mu(r)\sigma'^2(r)]. \qquad (18)
\end{aligned}$$

The conservation equation related to the additional source is

$$\Theta_1^{1'(\mathrm{eff})} - \frac{\xi'(r)}{2}(\Theta_0^{0(\mathrm{eff})} - \Theta_1^{1(\mathrm{eff})}) - \frac{2}{r}(\Theta_2^{2(\mathrm{eff})} - \Theta_1^{1(\mathrm{eff})}) = 0, \qquad (19)$$

where

$$\begin{aligned}
\Theta_0^{0(\mathrm{eff})} &= \frac{1}{\sigma}\left(\Theta_0^0+\frac{1}{2}\mu'(r)\sigma'(r)+\mu(r)\sigma''(r)+\frac{\omega_{BD}\mu(r)\sigma'^2(r)}{2\sigma(r)}+\frac{2\mu(r)\sigma'}{r}\right),\\
\Theta_1^{1(\mathrm{eff})} &= \frac{1}{\sigma}\left(\Theta_1^1+\frac{1}{2}\mu(r)\xi'(r)\sigma'(r)-\frac{\omega_{BD}\mu(r)\sigma'^2(r)}{2\sigma(r)}+\frac{2\mu(r)\sigma'(r)}{r}\right),\\
\Theta_2^{2(\mathrm{eff})} &= \frac{1}{\sigma}\left(\Theta_2^2+\frac{1}{2}\mu'(r)\sigma'(r)+\frac{1}{2}\mu(r)\xi'(r)\sigma'(r)+\mu(r)\sigma''(r)\right.\\
&+ \left.\frac{\omega_{BD}\mu(r)\sigma'^2(r)}{2\sigma(r)}+\frac{\mu(r)\sigma'(r)}{r}\right).
\end{aligned}$$

Equations (15) and (19) indicate that the MGD scheme conserves the decoupled sources (seed and additional) individually by not allowing exchange of energy. The matter variables of the original system are obtained by combining Equations (12)–(14) and (16)–(18). Thus, the density, radial and transverse pressure of the complete anisotropic solution are, respectively characterized as

$$\begin{aligned}
\rho &= \frac{-1}{2r^2\sigma(r)}[r\sigma(r)(r\sigma'(r)(\Upsilon\mu'(r)+\lambda'(r))+2\Upsilon\mu(r)(r\sigma''(r)+2\sigma'(r))\\
&+ 2\lambda(r)(r\sigma''(r)+2\sigma'(r)))+2\sigma^2(r)(\Upsilon r\mu'(r)+\Upsilon\mu(r)+r\lambda'(r)+\lambda(r)\\
&- 1)+r^2\omega_{BD}\sigma'^2(r)(\Upsilon\mu(r)+\lambda(r))-r^2\sigma(r)V(\sigma)], \qquad (20)\\
p_r &= \frac{1}{2r^2\sigma}[r^2\omega_{BD}\sigma'^2(r)(\Upsilon\mu(r)-\lambda(r))-r\sigma(r)(r\xi'(r)+4)\sigma'(r)(\Upsilon\mu(r)\\
&- \lambda(r))+2\sigma^2(r)(-\mu(r)(\Upsilon+\Upsilon r\xi'(r))+r\lambda(r)\xi'(r)+\lambda(r)-1)\\
&- r^2\sigma(r)V(\sigma)], \qquad (21)\\
p_\perp &= \frac{1}{4r\sigma(r)}[-2\sigma(r)(r\sigma'(r)(\Upsilon\mu'(r)-\lambda'(r))+\Upsilon\mu(r)((r\xi'(r)+2)\sigma'(r)\\
&+ 2r\sigma'')-\lambda(r)((r\xi'(r)+2)\sigma'(r)+2r\sigma''(r)))-\sigma^2(r)(\Upsilon\mu'(r)(r\xi'(r)\\
&+ 2)-\Upsilon\mu(2r\xi''(r)+r\xi'^2(r)+2\xi'(r))+2r\lambda(r)\xi''(r)+r\xi'(r)\lambda'(r)\\
&+ r\lambda(r)\xi'^2(r)+2\lambda(r)\xi'(r)+2\lambda'(r))+2r\omega_{BD}\sigma'^2(r)(\lambda(r)-\Upsilon\mu(r))\\
&- 2r\sigma(r)V(\sigma)]. \qquad (22)
\end{aligned}$$

The degrees of freedom can be reduced by employing well-behaved metric potentials to specify the matter variables of the system (12)–(14). The set incorporating the influence of Θ_δ^γ contains four undetermined functions (deformation function, Θ_0^0, Θ_1^1, Θ_2^2) and can be solved with the help of an additional constraint. Researchers have employed suitable forms of deformation function or an appropriate EoS to formulate a solution of the second set. Since the aim of this work is to develop quark star models, therefore we adopt MIT bag model as an EoS. The quarks within the strange star are classified into three flavors (f): up (u), strange (s) and down (d). We proceed by assuming that quark matter is non-interacting and massless in nature. The bag constant for massless quarks lies between 58.9 and 91.5 MeV/fm^3 [61]. The bag model defines the density and pressure of the star as

$$\rho=\sum_f \rho^f+\mathcal{B}, \quad p_r=\sum_f p^f-\mathcal{B}, \quad f=u,\ d,\ s, \qquad (23)$$

where ρ^f and p^f represent the density and pressure of each flavor, respectively. Kapusta [62] used the relation $\rho^f=3p^f$ to formulate the EoS for strange quark matter as

$$3p_r=\rho-4\mathcal{B}. \qquad (24)$$

Inserting Equations (20) and (21) in this EoS yields the following differential equation

$$\frac{1}{r\sigma(r)}\Big(2\sigma^2\big(\Upsilon r\mu'(r)+\Upsilon\mu(r)\big(3r\xi'(r)+4\big)+\lambda(r)\big(3r\xi'(r)+4\big)+r\lambda'(r)-4\big)+r\sigma(r)\big(\Upsilon r\mu'(r)\sigma'(r)+\Upsilon\mu(r)\big(\big(3r\xi'(r)+16\big)\sigma'(r)+2r\sigma''(r)\big)+3r\lambda(r)\xi'(r)\sigma'(r)+r\lambda'(r)\sigma'(r)+2r\lambda(r)\sigma''(r)+16\lambda(r)\sigma'(r)-4rV(\sigma)+8r\mathcal{B}\big)-2r^2\omega_{BD}\sigma'(r)^2(\Upsilon\mu(r)+\lambda(r))\Big)=0. \tag{25}$$

In the next section, we will develop two solutions for the isotropic sector and solve Equation (25) to obtain the corresponding deformation functions. A complete solution for the system (7)–(9) is computed by linearly combining the individual solutions of the two arrays. The potential function is chosen as $V(\sigma)=\frac{1}{2}m_\sigma^2\sigma^2$, where m_σ is the mass of the scalar field. Moreover, SBD theory is consistent with solar system observations for $m_\sigma > 10^{-4}$ (in dimensionless units). Therefore, we develop the decoupled quark star models corresponding to $m_\sigma = 0.001$.

4. Anisotropic Solutions

In this section, we assume two well-behaved radial metric components and utilize Karmarkar's embedding condition [63] to obtain the corresponding temporal metric functions related to the isotropic solution. A four-dimensional spherical spacetime belongs to embedding class-two as it can be embedded in a six-dimensional flat spacetime. However, it can be embedded in a five-dimensional flat spacetime only if it fulfils Karmarkar's criterion developed via Gauss–Codazi equations. The embedding of N-dimensional space in an $(N+1)$-dimensional pseudo-Euclidean space is allowed if the following conditions hold [64]

$$\mathcal{R}_{\gamma\delta\mu\upsilon}=2e\mathfrak{T}_{\gamma[\mu}\mathfrak{T}_{\upsilon]\delta}\quad\text{and}\quad\mathfrak{T}_{\gamma[\delta;\mu]}-\Gamma^{\lambda}_{\delta\mu}\mathfrak{T}_{\gamma\lambda}+\Gamma^{\lambda}_{\gamma[\delta}\mathfrak{T}_{\mu]\lambda}=0,$$

where $\mathfrak{T}_{\gamma\delta}$ and $\mathcal{R}_{\gamma\delta\mu\upsilon}$ are the co-efficients of second differential form and curvature tensor, respectively. Furthermore, $e=\pm1$. Karmarkar used this result to formulate a necessary and sufficient condition for an embedding class-one as

$$\mathcal{R}_{0101}\mathcal{R}_{2323}=\mathcal{R}_{1212}\mathcal{R}_{0303}+\mathcal{R}_{1202}\mathcal{R}_{1303}.$$

Applying the above condition to the metric in (ξ,λ)-frame (corresponding to $\Upsilon=0$) provides

$$(\lambda(r)-1)\lambda(r)\Big(2\xi''(r)+\xi'(r)^2\Big)-\lambda'(r)\xi'(r)=0. \tag{26}$$

4.1. Solution I

We assume that the isotropic solution is described by the radial metric component given as

$$\lambda(r)=\left(\frac{2\big(Ar^2+1\big)}{2-Ar^2}\right)^{-1}. \tag{27}$$

The Karmarkar's condition yields the temporal metric function as

$$\xi(r)=2\ln\left(G-\frac{Fr}{2\sqrt{\frac{Ar^2}{6-3Ar^2}}}\right),$$

where A, G and F are non-zero constants with $A>0$. It must be noted that the metric potential in Equation (27) is well-behaved, regular and singularity-free with finite behavior at the center. Maurya et al. [65] employed this ansatz to construct anisotropic stellar models. Recently, Baskey et al. [66] formulated a static stellar configuration by using this radial metric component in Karmarkar's condition. The unknown parameters in the metric

functions are determined by ensuring the continuity of first and second fundamental forms at the boundary (Σ) of internal and external spacetimes. The static vacuum in the exterior is defined by the Schwarzschild line element as

$$ds^2 = \frac{r-2M}{r}dt^2 - \frac{r}{r-2M}dr^2 - r^2 d\theta^2 - r^2 \sin^2\theta d\varphi^2, \tag{28}$$

where M denotes the mass. The form of corresponding scalar field has been determined by following the procedure in [42]. The constants are evaluated utilizing the conditions

$$\begin{aligned} (g^-_{\gamma\delta})_\Sigma &= (g^+_{\gamma\delta})_\Sigma, \quad (p_r)_\Sigma = 0, \\ (\sigma^-(r))_\Sigma &= (\sigma^+(r))_\Sigma, \quad (\sigma'^-(r))_\Sigma = (\sigma'^+(r))_\Sigma, \end{aligned}$$

as follows

$$A = -\frac{4M}{R^2(4M-3R)}, \tag{29}$$

$$G = \frac{5\sqrt{M}}{2\sqrt{R}\sqrt{-\frac{M}{2M-R}}}, \tag{30}$$

$$F = \frac{\sqrt{2}\sqrt{M}}{R^{3/2}}, \tag{31}$$

$$\begin{aligned} \omega_{BD} = & -(2M-R)\Big(\sqrt{3}FR\Big(4m_\sigma M^2 R\Big(AR^2+1\Big) - 4M\Big(AR^2\Big(m_\sigma R^2 \\ & + 2) + m_\sigma R^2 + 4\Big) + R^3\Big(A\Big(m_\sigma R^2 + 10\Big) + m_\sigma\Big)\Big) - 2G\sqrt{\frac{AR^2}{2-AR^2}} \\ & \times \Big(4m_\sigma M^2 R\Big(AR^2+1\Big) - 4M\Big(A\Big(m_\sigma R^4 + R^2\Big) + m_\sigma R^2 + 4\Big) + R^3 \\ & \times \Big(A\Big(m_\sigma R^2 + 6\Big) + m_\sigma\Big)\Big)\Big)\Big(4M^2\Big(AR^2-2\Big)\Big(\sqrt{3}FR \\ & - 2G\sqrt{\frac{AR^2}{2-AR^2}}\Big)\Big)^{-1}, \end{aligned} \tag{32}$$

where R denotes the radius of the spherical cosmic setup. The values of the constants are obtained for the star PSR J1903+327 ($M = 1.667 M_\odot$ and $R = 9.438$ km) [67]. Moreover, the constants G and F remain unchanged corresponding to the transformed metric potential. However, the values of A and ω_{BD} cannot be determined in the anisotropic scenario. There-

fore, we choose the values of A and ω_{BD} as given in Equations (29) and (32), respectively. The energy density and pressure components of the anisotropic analog turn out to be

$$\begin{aligned}
\rho &= \frac{-1}{2r^2\sigma}\Bigg(r\sigma(r)\Bigg(r\sigma'(r)\Bigg(\Upsilon\mu'(r)-\frac{3Ar}{(Ar^2+1)^2}\Bigg)+\frac{(2-Ar^2)}{Ar^2+1}(r\sigma''(r)\\
&+ 2\sigma')+2\Upsilon\mu(r)(r\sigma''+2\sigma'))+2\sigma^2\Bigg(r\Bigg(\Upsilon\mu'(r)-\frac{3Ar(Ar^2+3)}{2(Ar^2+1)^2}\Bigg)\\
&+ \Upsilon\mu(r))+r^2\omega_{BD}\sigma'(r)^2\Bigg(\frac{2-Ar^2}{2Ar^2+2}+\Upsilon\mu(r)\Bigg)-r^2\sigma(r)V(\sigma)\Bigg),\\
p_r &= \frac{1}{2r\sigma(r)}\Bigg(\sigma'(r)\Bigg(\frac{2-Ar^2}{2Ar^2+2}+\Upsilon\mu(r)\Bigg)(\sigma(r)(\zeta_1(r)+4)-r\omega_{BD}\sigma')\Bigg)\\
&+ \frac{\sigma(r)}{r^2}\Bigg(\mu(r)\Upsilon(\zeta_1+1)-\zeta_1(r)+\frac{2-Ar^2}{2Ar^2+2}-1\Bigg)-\frac{V(\sigma)}{2},\\
p_\perp &= \frac{\sigma(r)\zeta_2^{-1}(r)}{2(Ar^2-2)^2(Ar^2+1)^2}\Bigg(\Big(Ar^2-2\Big)\Big(Ar\Big(-3F^2r\Big(A^2r^4+3Ar^2\\
&- 10)+2\sqrt{3}FG\sqrt{\frac{Ar^2}{2-Ar^2}}\Big(A^2r^4+6Ar^2-16\Big)+12AG^2r\Bigg)\\
&+ 2\Upsilon\Big(Ar^2+1\Big)^2\mu'\Bigg(3F^2r\Big(Ar^2-1\Big)+\sqrt{3}FG\Big(4-3Ar^2\Big)\sqrt{\frac{Ar^2}{2-Ar^2}}\\
&- 2AG^2r\Big)\Big)+2\Upsilon AFr\Big(Ar^2-4\Big)\Big(Ar^2+1\Big)^2\mu(r)\Big(3Fr-2\sqrt{3}G\\
&\times \sqrt{\frac{Ar^2}{2-Ar^2}}\Bigg)\Bigg)+\Bigg(\frac{2-Ar^2}{2Ar^2+2}+\Upsilon\mu\Bigg)\Bigg(\frac{1}{2}\sigma'(r)\Bigg(\frac{\Upsilon\mu'(r)-\frac{3Ar}{(Ar^2+1)^2}}{\frac{2-Ar^2}{2Ar^2+2}+\Upsilon\mu(r)}\\
&+ \frac{2\sqrt{3}AFr^2}{(Ar^2-2)\sqrt{\zeta_2(r)}}+\frac{2}{r}\Bigg)+\sigma''(r)+\frac{\omega_{BD}\sigma'^2}{2\sigma(r)}\Bigg)-\frac{V(\sigma)}{2},
\end{aligned}$$

where $\zeta_1(r)=\frac{2\sqrt{3}AFr^3}{(Ar^2-2)\left(\sqrt{3}Fr-2G\sqrt{\frac{Ar^2}{2-Ar^2}}\right)}$ and $\zeta_2(r)=\left(\sqrt{3}Fr-2G\sqrt{\frac{Ar^2}{2-Ar^2}}\right)^2$. The massive scalar field and deformation function are computed numerically through Equations (10) and (25), respectively for $\mathcal{B}=60,70,80$ MeV/fm^3 and $\Upsilon=0.2,\ 0.9$. The corresponding initial conditions ($\sigma(0)=\sigma_c,\ \sigma'(0)=0,\ \mu(0)=\mu_c$) are presented in Table 1 where c indicates the value of the physical quantity at the center. Figure 1 indicates that the transformation does not disturb the regular behavior of metric potential. A stellar model is well-behaved if the matter variables are positive, finite at the center and decrease monotonically towards the boundary. As shown in Figures 2 and 3, the state determinants are maximum at the core and finite throughout for the considered values of bag constant and decoupling parameter. The anisotropy ($\Delta=p_\perp-p_r$) vanishes at $r=0$ and increases away from the center.

Table 1. Initial conditions corresponding to solution I for different values of the bag constant corresponding to $\Upsilon=0.2,\ 0.9$.

	$\mathcal{B}=60$ MeV/fm^3	$\mathcal{B}=70$ MeV/fm^3	$\mathcal{B}=80$ MeV/fm^3
σ_c	0.024	0.029	0.032
μ_c	0	0	0

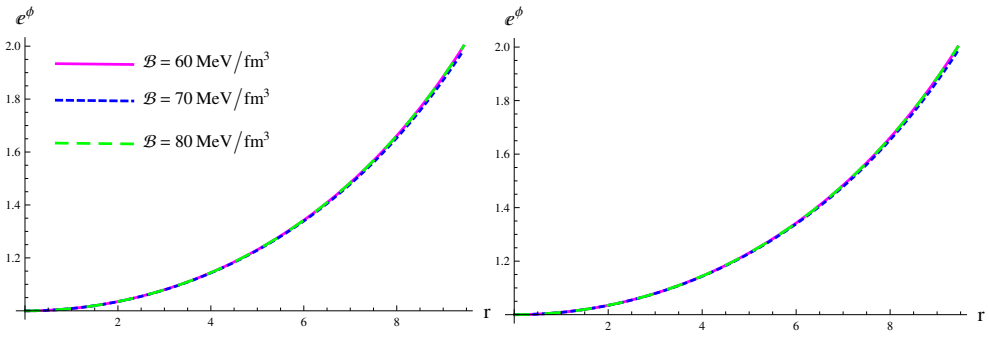


Figure 1. Plots of deformed radial metric components of solution I for $Y = 0.2$ (**left**) and $Y = 0.9$ (**right**).

State parameters describing celestial structures composed of normal matter must satisfy four energy conditions. These conditions are listed as [68]

$$\begin{aligned}
&\text{null energy condition:} \quad \rho + p_r \geq 0, \quad \rho + p_\perp \geq 0,\\
&\text{weak energy condition:} \quad \rho \geq 0, \quad \rho + p_r \geq 0, \quad \rho + p_\perp \geq 0,\\
&\text{strong energy condition:} \quad \rho + p_r + 2p_\perp \geq 0,\\
&\text{dominant energy condition:} \quad \rho - p_r \geq 0, \quad \rho - p_\perp \geq 0.
\end{aligned}$$

The density and pressure components related to the anisotropic setup are positive as indicated by Figures 2 and 3. Thus, the compact structure is consistent with the first three energy bounds. Figures 4 and 5 illustrate that the spherical system obeys the dominant energy condition as well which implies that the quark star model is viable for the considered values of Y.

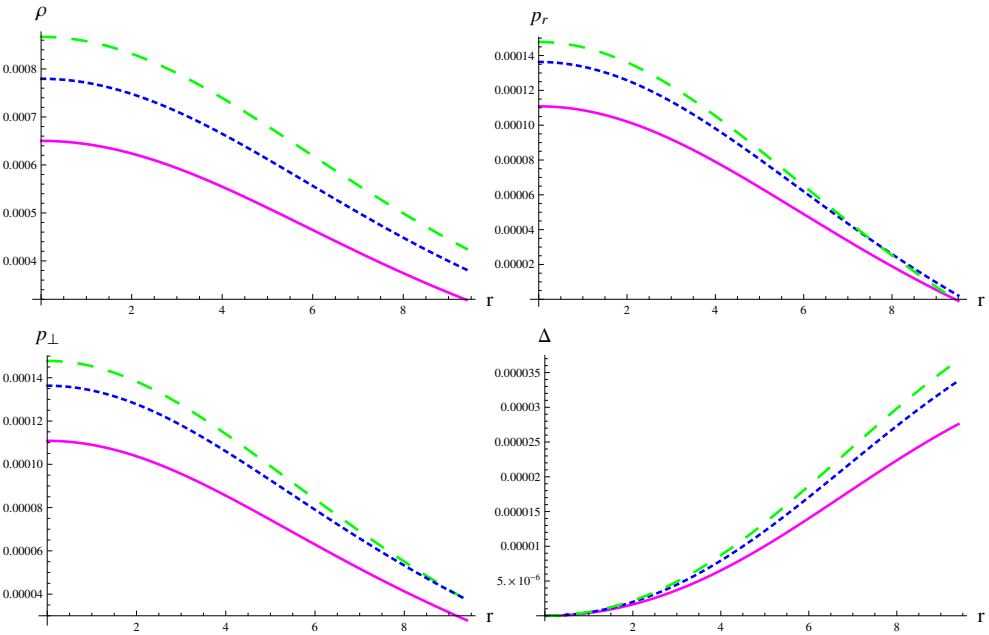


Figure 2. Behavior of ρ, p_r, $p_\perp$ (in km^{-2}) and Δ of solution I for $Y = 0.2$.

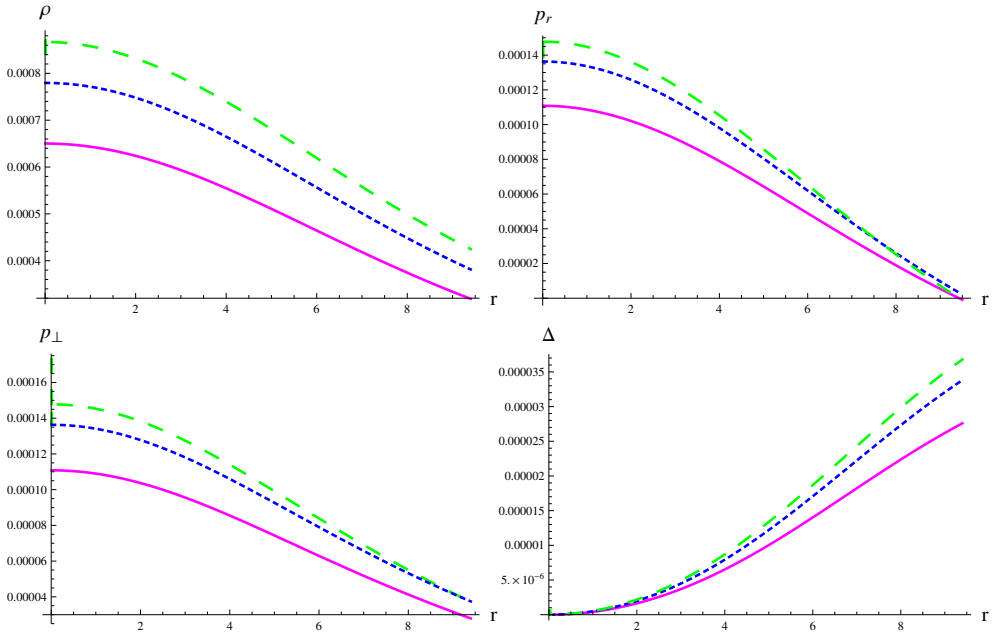


Figure 3. Behavior of ρ, p_r, $p_\perp$ (in km^{-2}) and Δ of solution I for Y $= 0.9$.

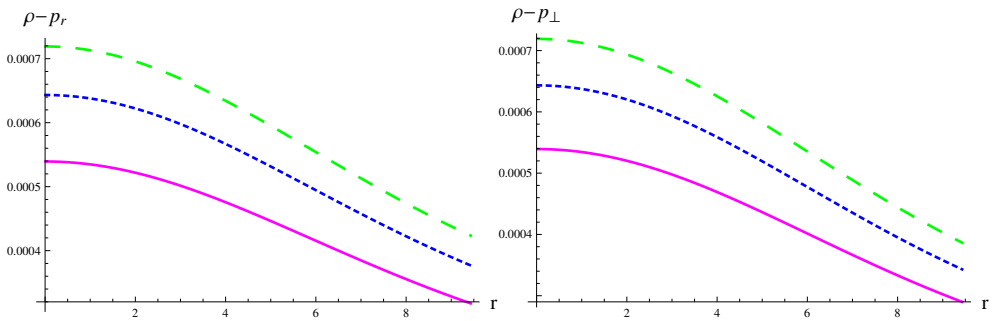


Figure 4. DEC for extended solution I for Y $= 0.2$.

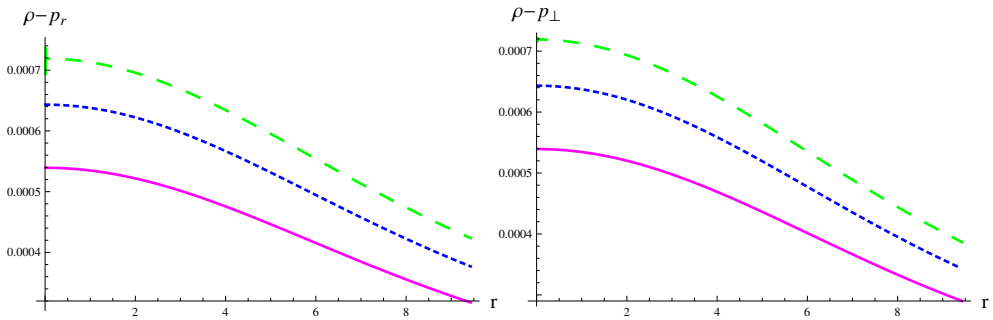


Figure 5. DEC for extended solution I for Y $= 0.9$.

The mass of the spherically symmetric configuration is computed by solving the differential equation

$$\frac{dm(r)}{dr} = \frac{1}{2}r^2\rho, \tag{33}$$

with the condition $m(0) = 0$. Furthermore, compact structures like quark stars have tightly packed atoms in the interior. The compactness ($u(r)$) of a spherical object is measured by its mass to radius ratio which must be less than 0.444 [69]. Figures 6 and 7 show that the anisotropic model fulfils the required criterion. Massive celestial structures possess

a strong gravitational field that bends electromagnetic waves. The strength of the force exerted on light is determined by gravitational redshift which is defined as

$$Z(r) = \frac{1-\sqrt{1-2u}}{\sqrt{1-2u}}.$$

The value of the redshift parameter for the anisotropic configuration lies within the admissable range, i.e., $Z(r) < 5.211$ [70] (refer to Figures 6 and 7). Moreover, the mass, compactness and redshift of the compact model increase corresponding to higher values of $\mathcal{B}$.

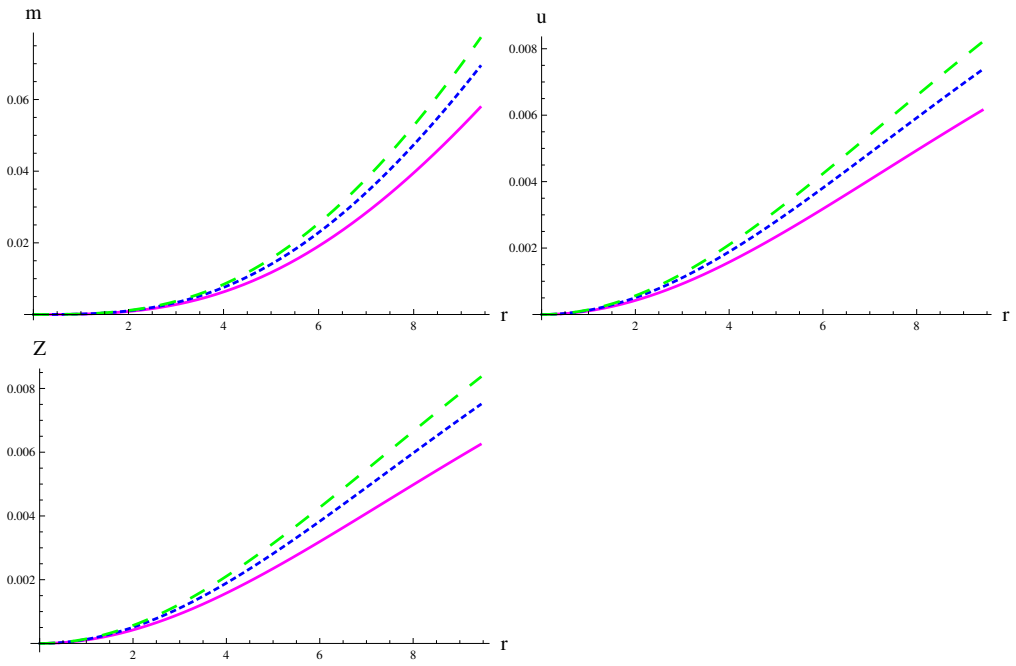


Figure 6. Behavior of m, u and Z corresponding to solution I for $Y = 0.2$.

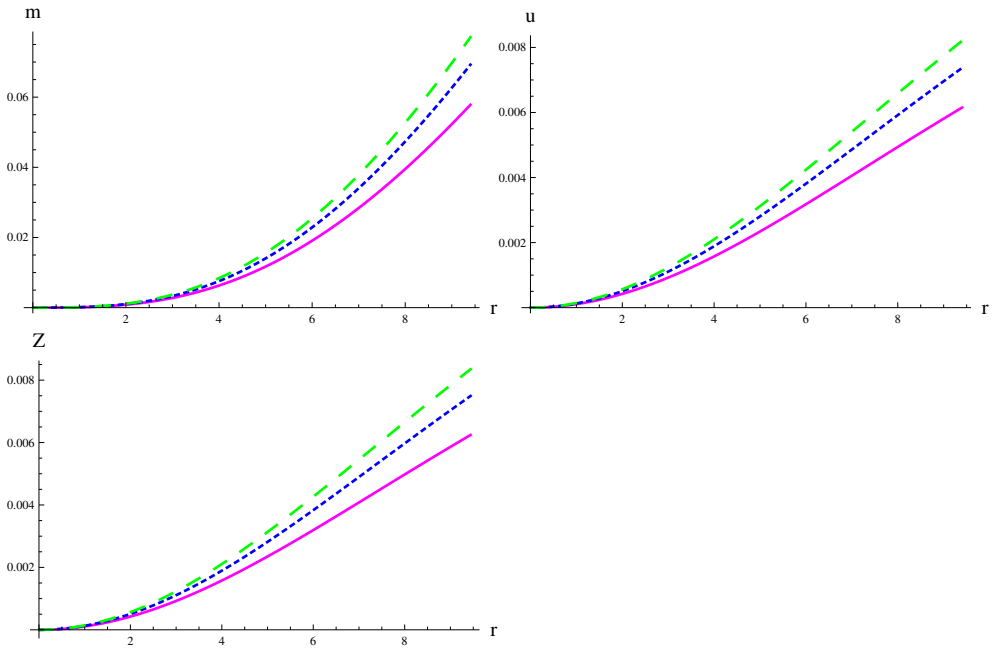


Figure 7. Behavior of m, u and Z corresponding to solution I for $Y = 0.9$.

The propagation rate of sound waves traveling through an anisotropic fluid distribution must be less than that of electromagnetic radiation, i.e., the components of sound speed ($(v_\perp^2 = \frac{dp_\perp}{d\rho})$ and $(v_r^2 = \frac{dp_r}{d\rho})$) must lie between 0 and 1. This criterion is used to check the stability of the stellar model and is known as the causality condition. Figures 8 and 9 exhibit that the anisotropic extension is stable for $Y = 0.2$ only. The spherical object is potentially stable if it adheres to Herrera's cracking criterion stated as $0 < |v_\perp^2 - v_r^2| < 1$. It is noted from Figures 8 and 9 that slight perturbations in the equilibrium of the stellar model do not lead to cracks within the system as the formulated solution fulfils the cracking condition for lower as well higher values of the decoupling parameter. Furthermore, the pressure of a compact model based on a stiff EoS increases rapidly in response to a change in density. Adiabatic index ($\Gamma = \frac{p_r+\rho}{p_r} v_r^2$) gauges the stiffness of the object and if $\Gamma > \frac{4}{3}$ then the system corresponds to a stiff EoS [71]. As displayed in Figures 8 and 9, the adiabatic index for the current setup is below the required limit close to the center but rises above $\frac{4}{3}$ after a short distance.

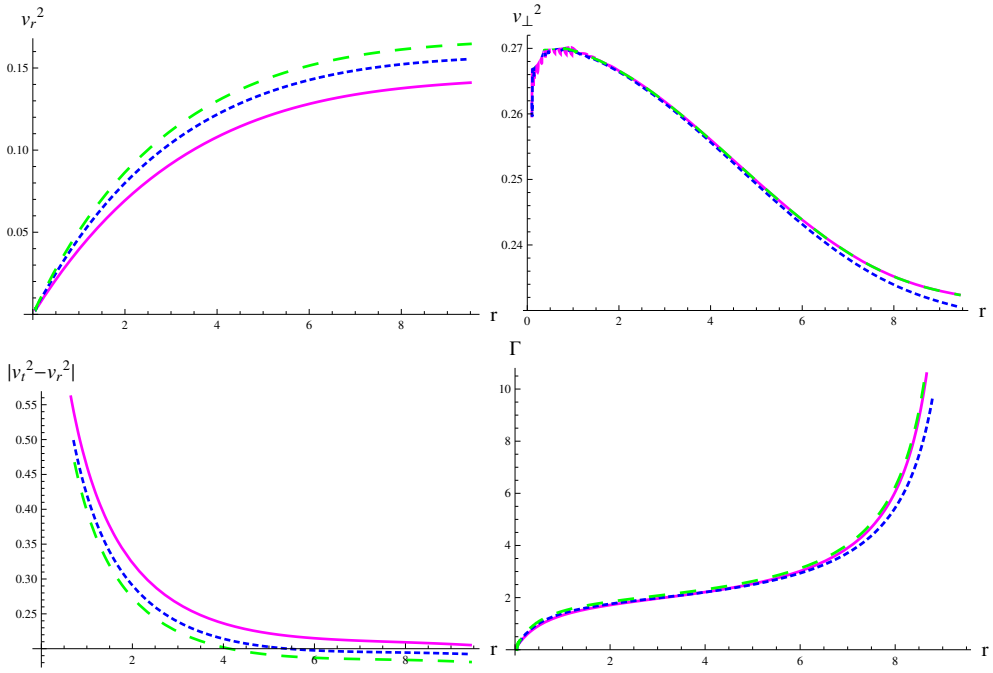


Figure 8. Plots of radial/tangential velocities, $|v_\perp^2 - v_r^2|$ and adiabatic index of extended solution I for $Y = 0.2$.

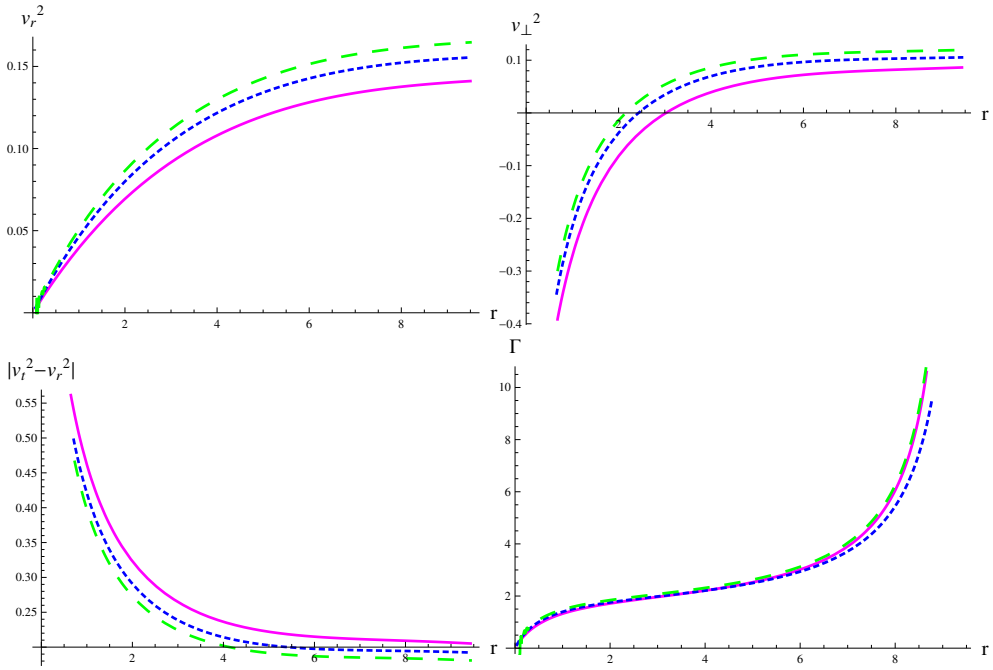


Figure 9. Plots of radial/tangential velocities, $|v_\perp^2 - v_r^2|$ and adiabatic index of extended solution I for Y = 0.9.

4.2. Solution II

The second isotropic solution is constructed by plugging the following radial metric in Karmarkar's condition

$$\lambda = \left(ar^2 \sin^2\left(br^2 + H\right) + 1\right)^{-1}, \tag{34}$$

which leads to

$$\xi(r) = 2\ln\left(D - \frac{\sqrt{a}B\cos\left(br^2 + H\right)}{2b}\right), \tag{35}$$

where a, b, B, D and H are constants. Mustafa et al. [72] recently proposed this physically valid ansatz to study dark stellar models in Rastall gravity. The unknown constants appearing in the spacetime are determined via matching with Schwarzschild vacuum solution as

$$a = -\frac{2M\csc^2\left(bR^2 + H\right)}{R^2(2M - R)}, \tag{36}$$

$$D = \frac{b\left(M\cot\left(bR^2 + H\right) + 2bR^2(R - 2M)\right)}{2R^2\sqrt{b^4R(R - 2M)}}, \tag{37}$$

$$B = \frac{b^2M\csc\left(bR^2 + H\right)}{\sqrt{2}R^2\sqrt{b^4R(R - 2M)}\sqrt{\frac{M\csc^2(bR^2+H)}{R^2(R-2M)}}}, \tag{38}$$

$$\begin{aligned}\omega_{BD} = {} & (2M - R)\Big(2b\Big(aDR^2(2M - R)(m_\sigma R(2M - R) - 4)\sin^2\Big(bR^2 \\ & + H) + 8\sqrt{a}BR^2(M - R)\sin\Big(bR^2 + H\Big) + D\Big(4m_\sigma M^2R - 4M \\ & \times \Big(m_\sigma R^2 + 4\Big) + m_\sigma R^3\Big)\Big) - \sqrt{a}B\cos\Big(bR^2 + H\Big)\Big(aR^2(2M - R) \\ & \times (m_\sigma R(2M - R) - 4)\sin^2\Big(bR^2 + H\Big) + 4m_\sigma M^2R - 4M\Big(m_\sigma R^2 \\ & + 4) + m_\sigma R^3\Big)\Big)\Big(8M^2\Big(2Db - \sqrt{a}B\cos\Big(bR^2 + H\Big)\Big)\Big)^{-1},\end{aligned} \tag{39}$$

where $C = \sqrt{a}BR^2(4M-3R)\cos\left(bR^2+H\right)+8bM$. The constants B and D remain the same after deformation whereas a, b, H and ω_{BD} appear as free parameters in the solution. The unknowns a and ω_{BD} are determined by Equations (36) and (39), respectively whereas we set $H = 1$ and $b = 0.01$. The field equations related to the considered setup take the form

$$\begin{aligned}
\rho &= -\frac{1}{2r^2\sigma(r)}\left(r\sigma(r)\left(r\sigma'(r)\left(\Upsilon\mu'(r)-\frac{2ar\left(\zeta_3(r)+br^2\sin(2\zeta_5)\right)}{\left(ar^2\zeta_3(r)+1\right)^2}\right)\right.\right.\\
&+ \left.\left.\frac{2\left(r\sigma''(r)+2\sigma'(r)\right)}{ar^2\zeta_3(r)+1}+2\Upsilon\mu(r)\left(r\sigma''(r)+2\sigma'(r)\right)\right)+2\sigma^2\left(r\left(\Upsilon\mu'(r)\right.\right.\right.\\
&- \left.\left.\left.\frac{ar\left(ar^2\zeta_3^2(r)+3\zeta_3(r)+2br^2\sin(2\zeta_5(r))\right)}{\left(ar^2\zeta_3(r)+1\right)^2}\right)+\Upsilon\mu(r)\right)+r^2\omega_{BD}\sigma'^2\\
&\times \left(\frac{1}{ar^2\zeta_3(r)+1}+\Upsilon\mu(r)\right)-r^2\sigma(r)V(\sigma)\Big),\\
p_r &= \frac{\sigma'(r)}{2r\sigma(r)}\left(\frac{1}{ar^2\zeta_3+1}+\Upsilon\mu\right)\left(\sigma\left(4-\frac{4\sqrt{a}bBr^2\sin(\zeta_5)}{\sqrt{a}B\cos(\zeta_5)-2Db}\right)\right.\\
&- \left.r\omega_{BD}\sigma'\right)+\frac{\sigma(r)}{r^2}\left(\mu(r)\left(\Upsilon-\frac{4\sqrt{a}\Upsilon bBr^2\sin(\zeta_5)}{\sqrt{a}B\cos(\zeta_5)-2Db}\right)+\frac{1}{ar^2\zeta_3(r)+1}\right.\\
&+ \left.\frac{4\sqrt{a}bBr^2\sin(\zeta_5)}{\left(ar^2\zeta_3(r)+1\right)\left(2Db-\sqrt{a}B\cos(\zeta_5)\right)}-1\right)-\frac{V(\sigma)}{2},
\end{aligned}$$

$$\begin{aligned}
p_\perp &= \frac{\sigma(r)}{2}\left(\frac{1}{ar^2\zeta_3(r)+1}+\Upsilon\mu(r)\right)\left(\frac{\Upsilon\mu'(r)\left(1-\frac{2\sqrt{a}bBr^2\sin(\zeta_5(r))}{\sqrt{a}B\zeta_4(r)-2Db}\right)}{r\left(\frac{1}{ar^2\zeta_3(r)+1}+\Upsilon\mu(r)\right)}\right.\\
&- \sqrt{a}\Big(2\left(ar^2\zeta_3+1\right)\left(\sqrt{a}B\zeta_4(r)-2Db\right)\left(\mu(r)\left(a\Upsilon r^2\zeta_3+\Upsilon\right)+1\right)\Big)^{-1}\\
&\times \left(-8\sqrt{a}Db^2r^2\sin(2\zeta_5)+4\sqrt{a}Db\cos(2\zeta_5)-4\sqrt{a}Db+4\Upsilon bB\mu(r)\right.\\
&\times \left(-ar^2\cos(2\zeta_5)+ar^2+2\right)^2\left(\sin(\zeta_5)+br^2\zeta_4(r)\right)+8abBr^2\sin(\zeta_5)\\
&+ \left.aB\zeta_4(r)-aB\cos(3\zeta_5)+16b^2Br^2\zeta_4(r)+16bB\sin(\zeta_5)\right)\Big)\\
&+ \left(\frac{1}{ar^2\zeta_3(r)+1}+\Upsilon\mu(r)\right)\left(\frac{1}{2}\sigma'(r)\left(-\frac{4\sqrt{a}bBr\sin(\zeta_5)}{\sqrt{a}B\zeta_4(r)-2Db}\right.\right.\\
&+ \left.\left.\frac{\Upsilon\mu'(r)-\frac{2ar\left(\zeta_3(r)+br^2\sin(2\zeta_5)\right)}{\left(ar^2\zeta_3(r)+1\right)^2}}{\frac{1}{ar^2\zeta_3+1}+\Upsilon\mu(r)}+\frac{2}{r}\right)+\sigma''(r)+\frac{\omega_{BD}\sigma'^2}{2\sigma(r)}\right)-\frac{V(\sigma)}{2},
\end{aligned}$$

where $\zeta_3(r) = \sin^2(\zeta_5)$, $\zeta_4(r) = \cos(\zeta_5)$ and $\zeta_5(r) = br^2 + H$. The scalar field and deformation function are computed through numerical solutions of Equations (10) and (25) for $m_\sigma = 0.001$, $\mathcal{B} = 60,\ 70,\ 80 MeV/fm^3$ and $\Upsilon = 0.2,\ 0.9$ corresponding to the the stellar model employed in solution I. Moreover, the central conditions ($\sigma(0) = \sigma_c$, $\sigma'(0) = 0$, $\mu(0) = \mu_c$) are mentioned in Table 2.

Table 2. Initial conditions corresponding to solution II for different values of the bag constant corresponding to Y = 0.2, 0.9.

	$\mathcal{B} = 60$ MeV/fm^3	$\mathcal{B} = 70$ MeV/fm^3	$\mathcal{B} = 80$ MeV/fm^3
σ_c	0.03	0.034	0.038
μ_c	0	0	0

The plots of radial metric component in Figure 10 show that the deformed metric function behaves regularly as well with finite value at the center for Y = 0.2, 0.9. The pressure components and energy density of the anisotropic quark star are positive and finite everywhere with a decreasing trend towards the stellar surface (refer to Figures 11 and 12). Moreover, the radial pressure vanishes at the boundary. A rise in the values of all matter variables is observed for higher values of the bag constant. The anisotropy of the extended solution is zero at the center and increases away from it. However, it starts to decline near the boundary indicating that radial pressure is more than the tangential pressure when $r \to R$. Figures 13 and 14 show that the quark model is viable for the considered values of the parameters as all energy conditions are satisfied. Higher values of the bag constant correspond to an increase in mass, compactness and redshift parameter as shown in Figures 15 and 16.

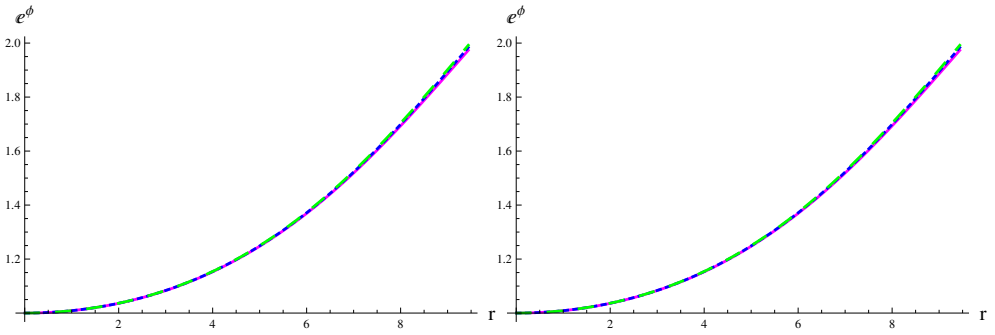


Figure 10. Plots of deformed radial metric components of anisotropic solution II for Y = 0.2 (**left**) and Y = 0.9 (**right**).

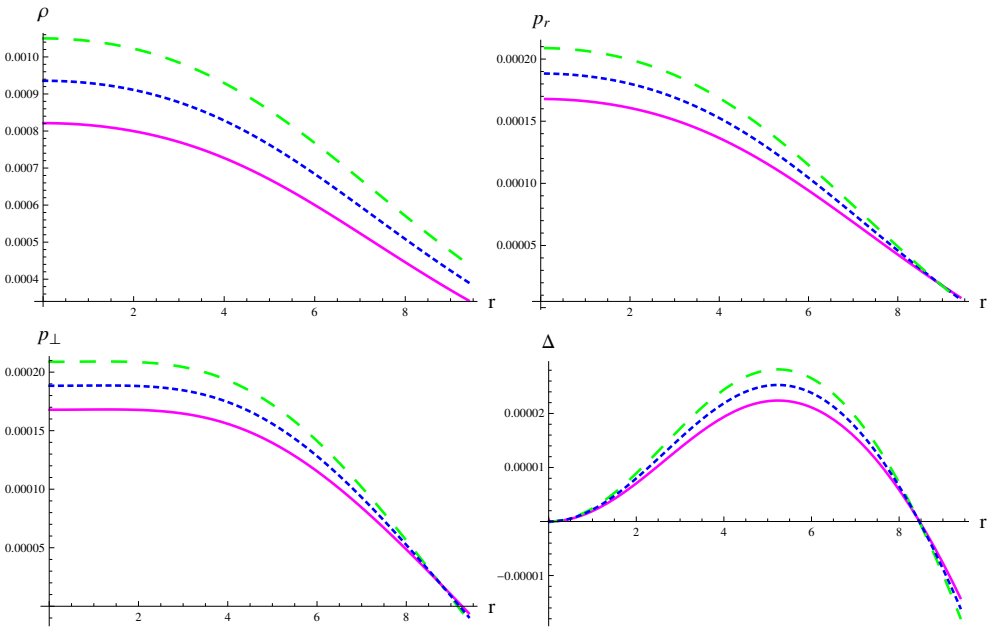


Figure 11. Behavior of ρ, p_r, $p_\perp$ (in km^{-2}) and Δ of anisotropic solution II for Y = 0.2.

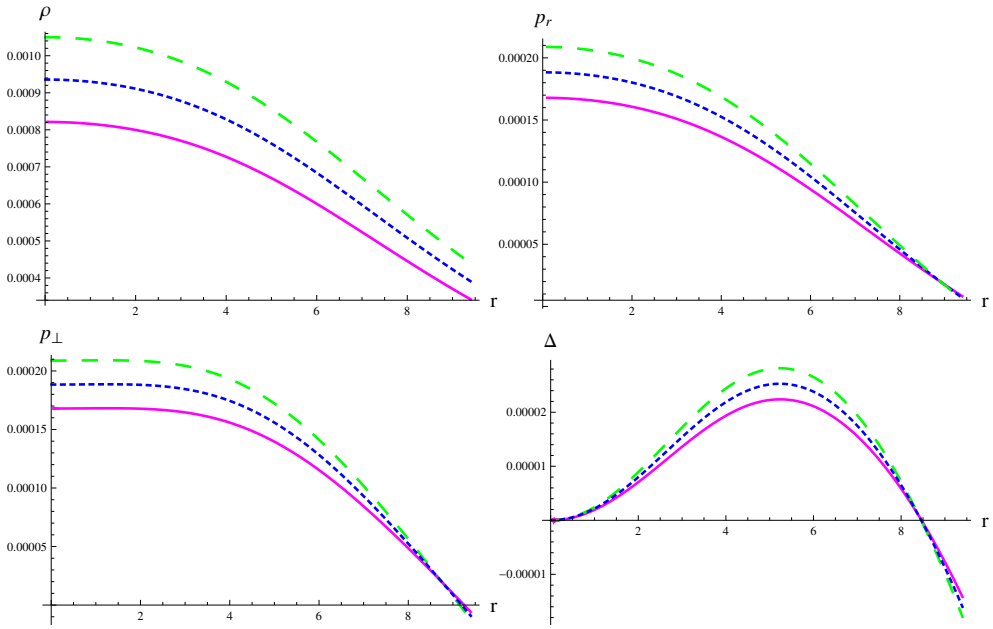


Figure 12. Behavior of ρ, p_r, $p_\perp$ (in km^{-2}) and Δ of anisotropic solution II for Y $= 0.9$.

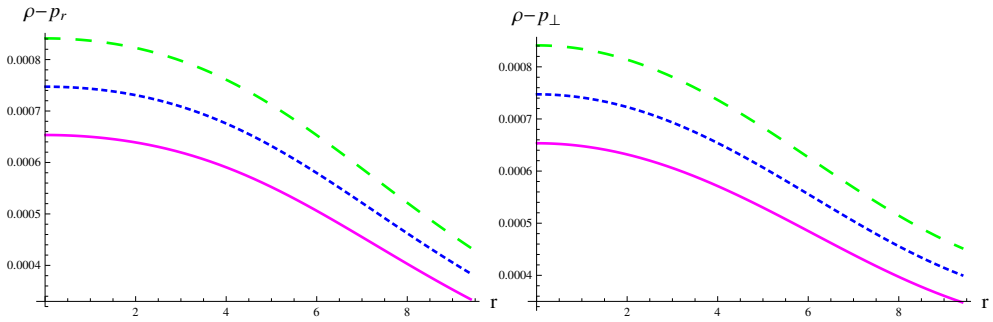


Figure 13. DEC for extended solution II for Y $= 0.2$.

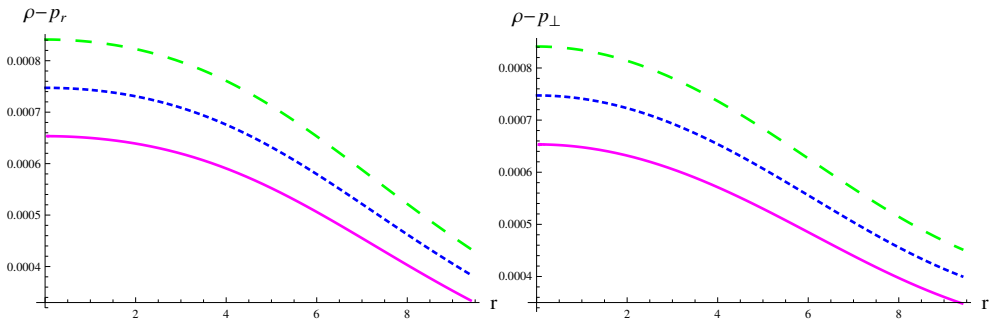


Figure 14. DEC for extended solution II for Y $= 0.9$.

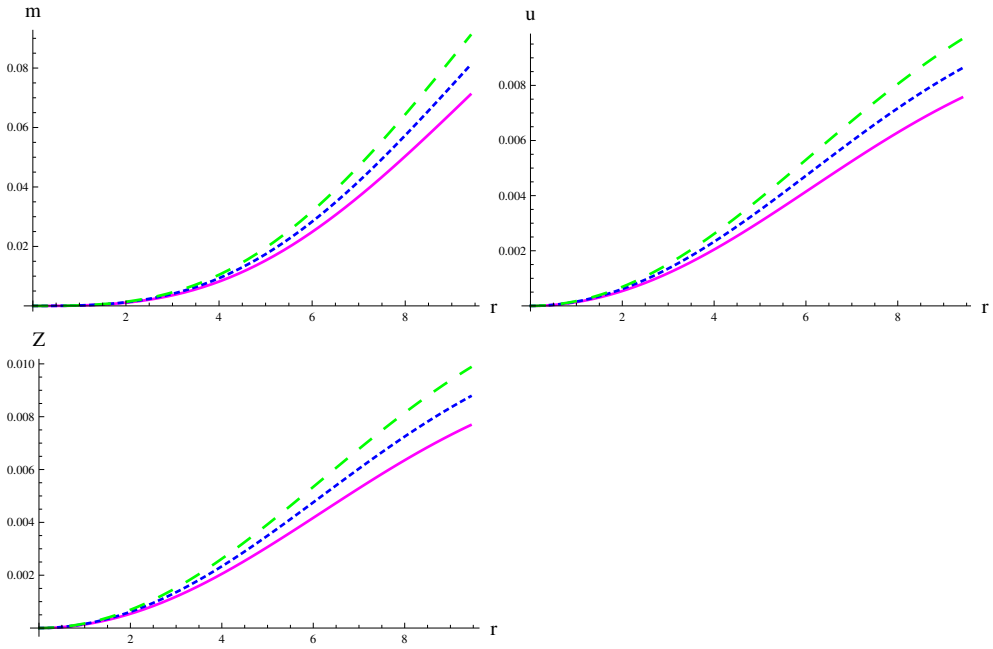


Figure 15. Behavior of m, u and Z corresponding to anisotropic solution II for $\mathrm{Y} = 0.2$.

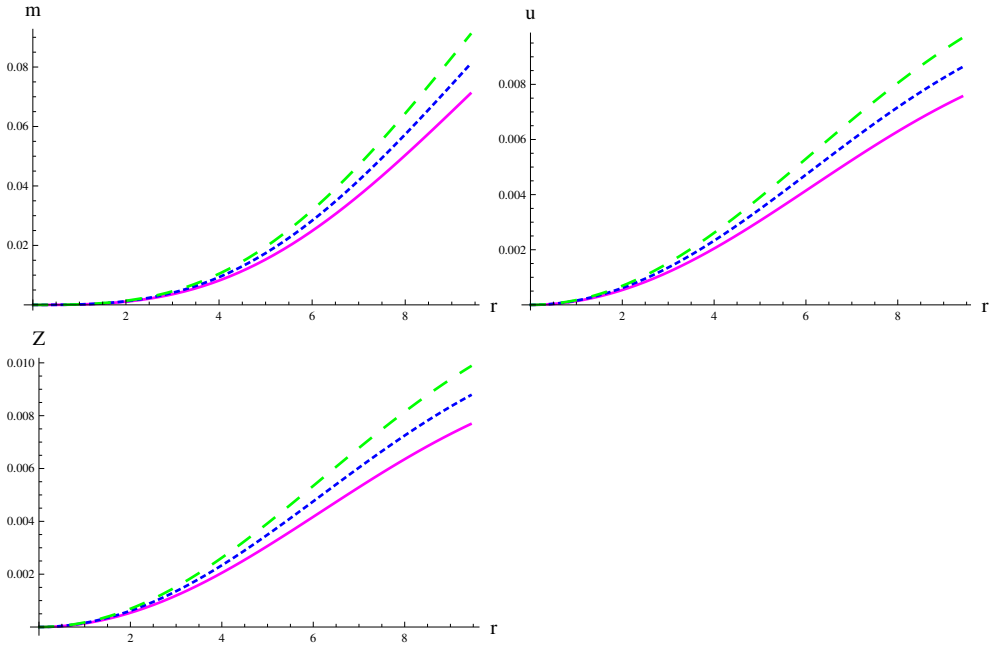


Figure 16. Behavior of m, u and Z corresponding to anisotropic solution II for $\mathrm{Y} = 0.9$.

Moreover, the redshift and compactness functions stay below the required limits. Figure 17 indicates that the extended version of the isotropic solution is stable according to causality and cracking criteria for $\mathrm{Y} = 0.2$. However, the causality condition is violated for $\mathrm{Y} = 0.9$ as $v_{\perp}^2 < 0$ (refer to Figure 18). The plots of adiabatic index exhibit that the anisotropic distribution is less stiff near the center. However, the values of Γ become greater than the required bound after a small distance from the center for both values of Y.

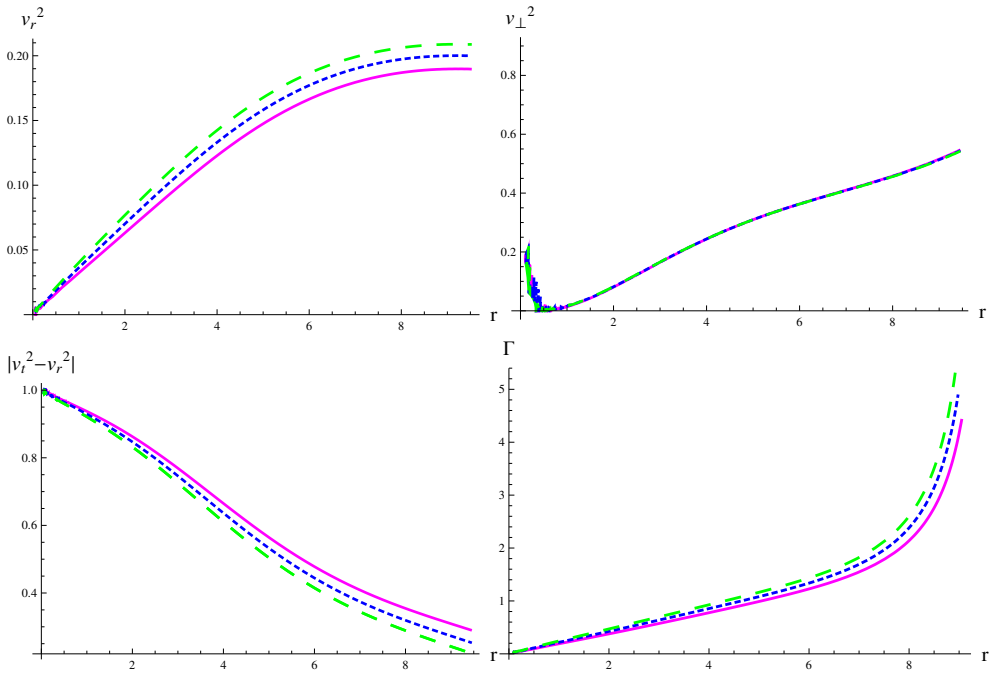


Figure 17. Plots of radial/tangential velocities, $|v_\perp^2 - v_r^2|$ and adiabatic index of extended solution II for Y = 0.2.

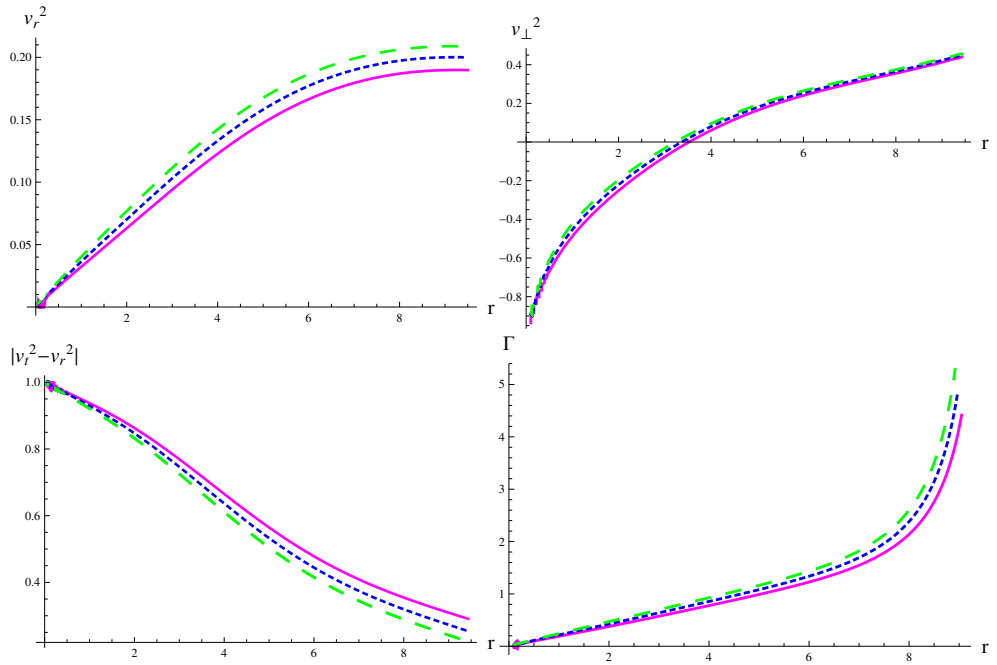


Figure 18. Plots of radial/tangential velocities, $|v_\perp^2 - v_r^2|$ and adiabatic index of extended solution II for Y = 0.9.

5. Conclusions

In order to comprehend the mechanism and evolution of the cosmos, it is essential to investigate the physical features of self-gravitating systems at different stages of its life-cycle. A strange star is one of the stellar remnants that is hypothesized to emerge from a neutron star. In this paper, we have developed anisotropic models representing strange quark stars by implementing the decoupling technique on SBD field equations. A linear deformation in the radial metric component has yielded two sets of field equations that incorporate one of the two sources (isotropic or additional). We have used Karmarkar's embedding

condition to develop two isotropic solutions corresponding to $\lambda = \ln\left(\frac{2(Ar^2+1)}{2-Ar^2}\right)$ and $\lambda = \ln\left(ar^2\sin^2\left(br^2+H\right)+1\right)$. We have employed these solutions to specify the set related to the isotropic source. The deformation function required to solve the second array has been obtained through an MIT bag model EoS. The matching of the interior and exterior spacetimes has specified the unknown constants in terms of mass and radius of the star. The scalar fields related to the anisotropic solutions have been obtained by numerically solving the wave equation for $V(\sigma) = \frac{1}{2}m_\sigma^2\sigma^2$, $m_\sigma = 0.001$, $\mathcal{B} = 60,\ 70,\ 80$ MeV/fm^3 and $Y = 0.2, 0.9$. Finally, the salient characteristics of the extended solutions have been analyzed graphically for the star PSR J1903+327.

The minimal geometric deformations in the metric functions of solutions I and II have provided well-behaved and regular stellar models. In both scenarios, the energy density and radial/transverse pressure have followed a monotonically decreasing trend after attaining the maximum value at the center. The anisotropy of the first solution has remained positive throughout which indicates the presence of a repulsive force directed outward. However, the anisotropy in solution II becomes negative near the stellar surface which implies that the direction as well as the nature of the force has changed. We have checked the viability of the constructed scenarios through four energy bounds. The spherical objects corresponding to solutions I and II have exhibited viable behavior implying the presence of normal matter in their interior for the considered values of the bag constant and the decoupling parameter.

It has been observed that higher values of the bag constant provide more massive quark stars with increased compactness and gravitational redshift. The gravitational redshift and compactness parameters have not violated their respective upper limits in any scenario. Finally, three stability criteria have been employed to examine the systems' response to perturbations in equilibrium. The analysis has shown that the extended solutions are potentially stable as they agree with Herrera's cracking criterion for $Y = 0.2,\ 0.9$. However, the causality condition is fulfilled for $Y = 0.2$ only as $v_\perp^2 < 0$ for $Y = 0.9$. Moreover, the plots of the adiabatic index have indicated that the cores of both solutions are less stiff. However, as distance from the center increases the fluid distribution becomes harder to compress. Thus, the decoupled quark models demonstrate physically viable and stable behavior for $\mathcal{B} = 60,\ 70,\ 80$ MeV/fm^3 and $Y = 0.2$. It is interesting to mention here that all the obtained results reduce to GR for $\sigma =$ constant and $\omega_{BD} \to \infty$.

Author Contributions: M.S. proposed the problem and finalized the manuscript while A.M. did the calculations and prepared the initial draft. All authors have read and agreed to the published version of the manuscript.

Funding: This research received no external funding.

Institutional Review Board Statement: No such data was used which requires IRB approval.

Informed Consent Statement: No such data was used in this work.

Data Availability Statement: The data supporting reported results can be found in [67].

Conflicts of Interest: The authors declare no conflict of interest.

References

1. Itoh, N. Hydrostatic equilibrium of hypothetical quark stars. *Prog. Theor. Phys.* **1970**, *44*, 291–292. [CrossRef]
2. Witten, E. Cosmic separation of phases. *Phys. Rev. D* **1984**, *30*, 272–285. [CrossRef]
3. Ofek, E.O.; Cameron, P.B.; Kasliwal, M.M.; Gal-Yam, A.; Rau, A.; Kulkarni, S.R.; Fraol, D.A.; Chandra, P.; Cenko, S.B.; Soderberg, A.M.; et al. SN2006gy: An extremely luminoue supernova in the galaxy NGC 1260. *Astrophys. J.* **2007**, *659*, L13. [CrossRef]
4. Bordbar, G.H.; Peivand, A.R. Computation of the structure of a magnetized strange quark star. *Res. Astron. Astrophys.* **2011**, *11*, 851–862. [CrossRef]
5. Abbott, B.P.; Abbott, R.; Abbott, T.D.; Acernese, F.; Ackley, K.; Adams, C.; Adams, T.; Addesso, P.; Adhikari, R.X.; Adya, V.B.; et al. GW170817: Observation of gravitational waves from a binary neutron star inspiral. *Phys. Rev. Lett.* **2017**, *119*, 161101. [CrossRef]
6. Abbott, B.P.; Abbott, R.; Abbott, T.D.; Abraham, S.; Acernese, F.; Ackley, K.; Adams, C.; Adhikari, R.X.; Adya, V.B.; Affeldt, C. et al. GW190425: Observation of a compact binary coalescence with total mass $\sim 3.4 M_\odot$. *Astrophys. J. Lett.* **2020**, *892*, L3. [CrossRef]

7. Haensel, P.; Zdunik, J.L.; Schaffer, R. Strange quark stars. *Astron. Astrophys.* **1986**, *160*, 121–128.
8. Cheng, K.S.; Dai, Z.G.; Lu, T. Strange stars and related astrophysical phenomena. *Int. J. Mod. Phys. D* **1998**, *7*, 139–176. [CrossRef]
9. Harko, T.; Mak, M.K. An exact anisotropic quark star model. *Chin. J. Astron. Astrophys.* **2002**, *2*, 248–259.
10. Arbañil, J.D.V.; Malheiro, M. Stability of charged quark stars. *AIP Conf. Proc.* **2015**, *1693*, 030007.
11. Bhar, P. Anisotropic compact star model: A brief study via embedding. *Eur. Phys. J. C* **2019**, *79*, 138. [CrossRef]
12. Ferreira, L.F.; da Rocha, R. Nucleons and higher spin baryon resonances: An AdS/Qcd configurational entropic incursion. *Phys. Rev. D* **2020**, *101*, 106002. [CrossRef]
13. Schwarzschild, K. On the gravitational field of a mass point according to Einstein's theory. *Math. Phys.* **1916**, *1916*, 189–196.
14. Herrera, L.; Santos, N.O. Local anisotropy in self-gravitating systems. *Phys. Rep.* **1997**, *286*, 53–130. [CrossRef]
15. Harko, T.; Mak, M.K. Anisotropic relativistic stellar models. *Annalen Phys.* **2002**, *11*, 3–13. [CrossRef]
16. Hossein, S.M.; Rahaman, F.; Naskar, J.; Kalam, M.; Ray, S. Anisotropic compact stars with variable cosmological constant. *Int. J. Mod. Phys. D* **2012**, *21*, 1250088. [CrossRef]
17. Paul, B.C.; Deb, R. Relativistic solutions of anisotropic compact objects. *Astrophys. Space Sci.* **2014**, *354*, 421–430. [CrossRef]
18. Ovalle, J. Decoupling gravitational sources in general relativity: From perfect to anisotropic fluids. *Phys. Rev. D* **2017**, *95*, 104019. [CrossRef]
19. Ovalle, J. Decopupling gravitational sources in general relativity: The extended case. *Phys. Lett. B* **2019**, *788*, 213–218. [CrossRef]
20. Ovalle, J.; Linares, F. Tolman IV solution in the Randall-Sundrum braneworld. *Phys. Rev. D* **2013**, *88*, 104026. [CrossRef]
21. Ovalle, J.; Casadio, R.; da Rocha, R.; Sotomayor, A. Anisotropic solutions by gravitational decoupling. *Eur. Phys. J. C* **2018**, *78*, 122. [CrossRef]
22. Gabbanelli, L.; Rincón, A.; Rubio, C. Gravitational decoupled anisotropies in compact stars. *Eur. Phys. J. C* **2018**, *78*, 370. [CrossRef]
23. Estrada, M.; Tello-Ortiz, F. A new family of analytical anisotropic solutions by gravitational decoupling. *Eur. Phys. J. C* **2018**, *133*, 453. [CrossRef]
24. Sharif, M.; Sadiq, S. Gravitational decoupled charged anisotropic spherical solutions. *Eur. Phys. J. C* **2018**, *78*, 410. [CrossRef]
25. Gabbanelli, L.; Ovalle, J.; Sotomayor, A.; Stuchlik, Z.; Casadio, R. A causal Schwarzschild-de Sitter interior solution by gravitational decoupling. *Eur. Phys. J. C* **2019**, *79*, 486. [CrossRef]
26. Contreras, E. Gravitational decoupling in 2+1 dimensional spacetime with cosmological term. *Class. Quantum Gravity* **2019**, *36*, 095004. [CrossRef]
27. Contreras, E.; Bargueño, P. Extended gravitational decoupling in 2+1 dimensional spacetimes. *Class. Quantum Gravity* **2019**, *36*, 215009. [CrossRef]
28. Singh, K.N.; Maurya, S.K.; Jasim, M.K.; Rahaman, F. Minimally deformed anisotropic model of class-one spacetime by gravitational decoupling. *Eur. Phys. J. C* **2019** *79*, 851. [CrossRef]
29. Hensh, S.; Stuchlik, Z. Anisotropic Tolman VII solution by gravitational decoupling. *Eur. Phys. J. C* **2019**, *79*, 834. [CrossRef]
30. Sharif, M.; Ama-Tul-Mughani, Q. Study of (1+2)-dimensional charged string cloud with minimal geometric deformation. *Int. J. Geom. Methods Mod. Phys.* **2019**, *16*, 1950187. [CrossRef]
31. Sharif, M.; Ama-Tul-Mughani, Q. Gravitational decoupled solutions of axial string cosmology. *Mod. Phys. Lett. A* **2020**, *35*, 2050091. [CrossRef]
32. Cedeño, F.X.L.; Contreras, E. Gravitational decoupling in cosmology. *Phys. Dark Universe* **2020**, *28*, 100543. [CrossRef]
33. Contreras, E.; Ovalle, J.; Casadio, R. Gravitational decoupling for axially symmetric systems and rotating black holes. *Phys. Rev. D* **2021**, *103*, 044020. [CrossRef]
34. Meert, P.; da Rocha, R. Probing the minimal geometric deformation with trace and Weyl anomalies. *Nucl. Phys. B* **2021**, *967*, 115420. [CrossRef]
35. Dirac, P.A.M. The cosmological constants. *Nature* **1937**, *139*, 323. [CrossRef]
36. Dirac, P.A.M. A new basis for cosmology. *Proc. R. Soc. Lond. A* **1938**, *165*, 199–208. [CrossRef]
37. Brans, C.; Dicke, R.H. Mach's principle and a relativistic theory of gravitation. *Phys. Rev.* **1961**, *124*, 925–935. [CrossRef]
38. Will, C.M. Theory and experiment in gravitational physics. *Living Rev. Rel.* **2001**, *4*, 4. [CrossRef]
39. Weinberg, E.J. Some problems with extended inflation. *Phys. Rev. D* **1989**, *40*, 3950. [CrossRef]
40. Perivolaropoulos, L. PPN parameter γ and solar system constraints of massive Brans-Dicke theories. *Phys. Rev. D* **2010**, *81*, 047501. [CrossRef]
41. Buchdahl, H.A. Static solutions of the Brans-Dicke equations. *Int. J. Theor. Phys.* **1972**, *6*, 407–412. [CrossRef]
42. Bruckman, W.F.; Kazes, E. Properties of the solutions of cold ultradense configurations in the Brans-Dicke theory. *Phys. Rev. D* **1977**, *16*, 2. [CrossRef]
43. Singh, T.; Rai, L.N. Stationary axially symmetric Brans-Dicke Maxwell fields. *Gen. Relat. Gravit.* **1979**, *11*, 37–43. [CrossRef]
44. Krori, K.D.; Bhattacharjee, D.R. Demiański-type metric in Brans-Dicke theory. *J. Math. Phys.* **1982**, *23*, 1846–1847. [CrossRef]
45. Yazadjiev, S.S.; Doneva, D.D; Popchev, D. Slowly rotating neutron stars in scalar-tensor theories with a massive scalar field. *Phys. Rev. D* **2016**, *93*, 084038. [CrossRef]
46. Doneva, D.D.; Yazadjiev, S.S. Rapidly rotating neutron stars with a massive scalar field-structure and universal relations. *J. Cosmol. Astropart. Phys.* **2016**, *11*, 019. [CrossRef]

47. Staykov, K.V.; Popchev, D.; Doneva, D.D.; Yazadjiev, S.S. Static and slowly rotating neutron stars in scalar-tensor theory with a massive scalar field. *Eur. Phys. J. C* **2018**, *78*, 586. [CrossRef]
48. Popchev, D.; Staykov, K.V.; Doneva, D.D.; Yazadjiev, S.S. Moment of inertia-mass universal relations for neutron stars in scalar-tensor theory with self-interacting massive scalar field. *Eur. Phys. J. C* **2019**, *79*, 178. [CrossRef]
49. Sharif, M.; Majid, A. Anisotropic strange stars through embedding technique in massive Brans-Dicke gravity. *Eur. Phys. J. Plus* **2020**, *135*, 558. [CrossRef]
50. Sharif, M.; Majid, A. Quark stars in massive Brans-Dicke gravity with Tolman-Kuchowicz spacetime. *Universe* **2020**, *6*, 124.
51. Sharif, M.; Saba, S. Gravitational decoupled anisotropic solutions in $f(\mathcal{G})$ gravity. *Eur. Phys. J. C* **2018**, *78*, 921. [CrossRef]
52. Sharif, M.; Waseem, A. Anisotropic spherical solutions by gravitational decoupling in $f(\mathcal{R})$ gravity. *Ann. Phys.* **2019**, *405*, 14–28. [CrossRef]
53. Sharif, M.; Waseem, A. Effects of charge on gravitational decoupled anisotropic solutions in $f(\mathcal{R})$ gravity. *Chin. J. Phys.* **2019**, *60*, 426–439. [CrossRef]
54. Sharif, M.; Majid, A. Anisotropic compact stars in self-interacting Brans-Dicke gravity. *Astrophys. Space Sci.* **2020**, *365*, 42. [CrossRef]
55. Sharif, M.; Majid, A. Decoupled anisotropic spheres in self-interacting Brans-Dicke gravity. *Chin. J. Phys.* **2020**, *68*, 406–418. [CrossRef]
56. Maurya, S.K.; Tello-Ortiz, F.: Charged anisotropic compact star in $f(\mathcal{R},T)$ gravity. *Phys. Dark Universe* **2020**, *27*, 100442. [CrossRef]
57. Sharif, M.; Majid, A. Extended gravitaional decoupled solutions in self-interacting Brans-Dicke gravity. *Phys. Dark Universe* **2020**, *30*, 100610. [CrossRef]
58. Maurya, S.K.; Errehymy, A.; Sing, K.N.; Tello-Ortiz, F; Daoud, M. Gravitational decoupling minimal geometric deformation model in modified $f(\mathcal{R},T)$ gravity. *Phys. Dark Universe* **2020**, *30*, 100640. [CrossRef]
59. Maurya, S.K.; Tello-Ortiz, F; Ray, S. Decoupling gravitational sources in $f(\mathcal{R},T)$ gravity under class I spacetime. *Phys. Dark Universe* **2021**, *31*, 100753. [CrossRef]
60. Azmat, H.; Zubair, M. An anisotropic version of Tolman VII solution in $f(\mathcal{R},T)$ gravity via gravitational decoupling MGD approach. *Eur. Phys. J. Plus* **2021**, *136*, 112. [CrossRef]
61. Farhi, E.; Jaffe, R.L. Strange matter. *Phys. Rev. D* **1984**, *30*, 2379. [CrossRef]
62. Kapusta, J.I. *Finite-Temperature Field Theory*; 2nd ed.; Cambridge University Press; Cambridge, UK, 2011.
63. Karmarkar, K.R. Gravitational metrics of spherical symmetry and class one. *Proc. Ind. Acad. Sci. A* **1948**, *27*, 56. [CrossRef]
64. Eisenhart, L.P. *Riemannian Geometry*, 1st ed.; Princeton University Press: Princeton, NJ, USA, 1926.
65. Maurya, S.K.; Gupta, Y.K.; Dayanandan, B.; Jasim, M.K.; Al-jamel, A. Relativistic anisotropic models for compact star with equation of state $p = f(p)$. *Int. J. Mod. Phys. D* **2017**, *26*, 1750002. [CrossRef]
66. Baskey, L.; Das, S.; Rahaman, F. An analytical anisotropic compact stellar model of embedding class I. *Mod. Phys. Lett. A* **2021**, *36*, 2150028. [CrossRef]
67. Gangopadhay, T.; Ray, S.; Xiand-Dong, L.; Jishnu, D. Strange star equation of state fits the refined mass measurement of 12 pulsaurs and predictes their radii. *Mon. Not. R. Soc.* **2013**, *431*, 3216–3221. [CrossRef]
68. Atazadeh, K.; Khaleghi, A.; Sepangi, H.R.; Tavakoli, Y. Energy conditions in $f(\mathcal{R})$ gravity and Brans-Dicke theories. *Int. J. Mod. Phys. D* **2009**, *18*, 1101–1111. [CrossRef]
69. Buchdahl, H.A. General relativistic fluid spheres. *Phys. Rev.* **1959**, *116*, 1027–1034. [CrossRef]
70. Ivanov, B.V. Maximum bounds on the surface redshift of anisotropic stars. *Phys. Rev. D* **2002**, *65*, 104011. [CrossRef]
71. Heintzmann, H.; Hillebrandt, W. Neutron stars with an anisotropic equation of state: Mass, redshift and stability. *Astron. Astrophys.* **1975**, *24*, 51–55.
72. Mustafa, G.; Hussain, I.; Shamir, M.F.; Tie-Cheng, X. Realistic and dark stellar models via embedding approach in Rastall gravity. *Phys. Scr.* **2021**, *96*, 045009. [CrossRef]